



Controllability Properties of Solar Sails

Alesia Herasimenka,*[✉] Lamberto Dell'Elce,[†] Jean-Baptiste Caillau,[‡] and Jean-Baptiste Pomet[§]
Université Côte d'Azur, 06108, France

<https://doi.org/10.2514/1.G007250>

Trajectory design and stationkeeping of solar sails about a celestial body can be formulated as control problems with positivity constraints. Specifically, when reemitted radiation is neglected and the sail is modeled as a flat surface, which are reasonable assumptions for control purposes, the force generated by the solar radiation pressure is contained in a pointed convex cone of revolution with the axis in the sun–satellite direction. Therefore, classical approaches to infer controllability based on the Lie algebra rank condition do not apply to these problems. This study offers a novel condition to decide on controllability of control systems with positivity constraints. This condition is effective because it can be verified by solving an auxiliary convex optimization problem for which reliable numerical methods are available. A crucial ingredient of this approach is the theory of positive trigonometric polynomials. The practical interest of this condition is the assessment of a minimum requirement on the optical properties of the sail, which may be of use for mission design purposes.

I. Introduction

SOLAR sails offer a propellantless solution to perform interplanetary transfers, planet escapes, and deorbiting maneuvers by leveraging on solar radiation pressure (SRP) ([1] Chap. 2). Although very few solar-sail missions have been launched to this date, the possibility to use SRP as an inexhaustible source of propulsion has attracted the interest of researchers in the last decades, therefore leading to several contributions on the guidance and control of solar sails. Specifically, a large body of literature focuses on the mathematical formulation and numerical solution of optimal control problems (OCPs) to find minimum-time interplanetary transfer trajectories using optimization techniques with locally optimal control laws [2,3], indirect methods [4], or even neural networks [5]. In addition, several contributions investigate locally optimal steering laws to maximize the instantaneous rate of change of a desired orbital element, with particular focus on the increase of the semimajor axis for orbit raising [6] or decrease of the perigee altitude for deorbiting applications [7]. Classical feedback algorithms are also used to find suboptimal trajectories: for instance, the Q-law algorithm in Ref. [8]. Direct methods are often preferred to find the numerical solution of OCP for solar-sail transfers [9–11]. This is due to the fact that direct methods do not require an initial guess of the adjoint variables, as opposed to indirect techniques that, for this reason, have been used in few studies [12–16].

Interestingly, very few studies on the controllability of solar sails are available to date, although an analysis of the reachable set of passive sails was discussed in Ref. [17]. Most often, the solutions of two-point boundary value problems coming, for instance, from optimal control are investigated without assessing beforehand whether the targeted final state is within the reachable set of the control system from the initial point, i.e., if the sail is capable of achieving the desired maneuver. Although exhibiting a solution of the two-point boundary value problem proves reachability as a side

result, it is of paramount importance to certify noncontrollability and seek for solutions only when controllability holds.

A major difficulty in assessing the controllability of an SRP-actuated system is that the sail cannot generate a force with a positive component toward the direction of the sun, and so the classical tools of geometric control theory cannot be used. For example, one of the requirements for the controllability is that the Lie algebra of the system must have full rank. It is indeed satisfied by the solar sail, unless a fully absorptive surface model of the sail is considered, which is physically unfeasible. However, even in this case, theory requires that the control set is a neighborhood of the origin, implying that both positive and negative controls should be generated, and so it is not sufficient to analyze solar sails. This aspect is particularly critical when considering a nonideal sail model for which the sail is assumed to be flat but not perfectly reflective. In this case, the control set is contained inside a strictly convex cone of revolution, for which the angle depends on the optical properties of the sail.

The main contribution of the paper consists of a controllability check for nonideal solar sails in planet-centered orbits. This requirement is aimed at assessing whether a nonideal solar sail with given optical parameters is capable of decreasing or increasing all possible functions of the Keplerian integrals of motion (e.g., Keplerian or equinoctial orbital elements) over an orbital period. In other words, we propose a methodology allowing us to verify if a solar sail can change the orbit in any desirable way. Given some optical properties, a convex cone containing all possible directions of the SRP force is first defined. Then, the necessary controllability condition we propose is verified by means of a worst-case optimization problem characterized by a finite number of design variables and a two-parameter family of inequality constraints, namely, the clock angle of the convex cone associated to the control set and the true anomaly of the sail. A numerical solution of this semi-infinite problem is achieved by leveraging on the formalism of squared functional systems ([18] Chap. 17, [19] Chap. 3) to exactly enforce inequality constraints for all values of the true anomaly and clock angle. No discretization is performed to solve the problem numerically. Eventually, the semi-infinite problem is recast into a finite-dimensional convex programming problem with a finite number of linear matrix inequalities (LMIs) and a unique well-defined solution. Nonsatisfaction of the condition entails some local noncontrollability of the system for the given value of the cone angle (and consequently of the optical properties) and orbital conditions. Hence, a fine numerical analysis covering the entire phase space of orbital elements is carried out to determine the minimum cone angle for a large range of orbits. It is shown that a universal (namely, planet-independent) minimum cone angle exists that satisfies the condition for all orbits. Its value is about 60 deg (note that 0 and 90 deg correspond to fully absorptive and perfectly reflective sails, respectively). The result indicates that the sail does not have to be ideal to satisfy the requirement.

Received 17 September 2022; revision received 29 November 2022; accepted for publication 1 December 2022; published online 31 January 2023. Copyright © 2022 by the authors. Published by the American Institute of Aeronautics and Astronautics, Inc., with permission. All requests for copying and permission to reprint should be submitted to CCC at www.copyright.com; employ the eISSN 1533-3884 to initiate your request. See also AIAA Rights and Permissions www.aiaa.org/randp.

*Ph.D. Student, Université Côte d'Azur, CNRS, INRIA, LJAD, MCTAO; alesia.herasimenka@univ-cotedazur.fr.

[†]Researcher, Inria center of Université Côte d'Azur, CNRS, LJAD, MCTAO; lamberto.dell-elce@inria.fr.

[‡]Professor, Université Côte d'Azur, CNRS, INRIA, LJAD, MCTAO; jean-baptiste.caillau@univ-cotedazur.fr.

[§]Senior Researcher, Inria center of Université Côte d'Azur, CNRS, LJAD, MCTAO; jean-baptiste.pomet@inria.fr.

The methodology is based only on the conical hull of the control set, regardless of the specific source of nonideality of the sail (e.g., specular reflection, diffuse reflection, or reemitted radiation) ([1] Chap. 2). This result can be used to provide insight into the controllability of the sail during its lifetime, owing to the degradation of its optical properties discussed in Ref. [20] and may support the design of real-life missions by serving as a minimal requirement to be satisfied.

Section II introduces the solar-sail dynamical model, the geometry of the problem, the equations of motion, and the assumptions used in this work. Section III outlines the novel condition for investigating the local controllability of systems with peculiar constraints on the solar-sail control set. An efficient numerical methodology based on convex programming to evaluate the aforementioned condition is detailed in Sec. IV. Finally, this methodology is extensively used in Sec. V to deduce minimal requirements on the optical properties of solar sails, and an example of stationkeeping around the moon is provided. The controllability of heliocentric orbits is briefly discussed as well.

II. Dynamics of a Solar Sail

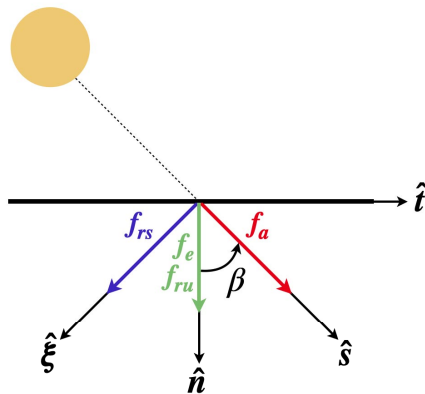
A. Force Model

Solar sails use SRP as propulsive means for orbit control and maneuvering. The SRP is generated by the interaction between photons and the surface of the sail, and its magnitude depends on the sun-sail distance r . Specifically, denoting by $\Phi_{SR} = 1367 \text{ W} \cdot \text{m}^{-2}$ the solar flux at $r_{\oplus} = 1 \text{ AU}$ (astronomical unit) from the sun and by c the speed of light, a simple model for the SRP is given by ([21] Chap. 3)

$$P_{SR} = \frac{\Phi_{SR}}{c} \left(\frac{r_{\oplus}}{r} \right)^2$$

A flat sail with surface A and mass m is considered in this work. The resulting force depends on various optical and geometrical properties of the sail; and it is obtained by summing up the force contributions of the incoming, reflected, and thermal radiations, namely, f_a , f_r , and f_e . In addition, the force given by the reflected radiation is divided into specular and diffuse components, f_{rs} and f_{ru} , respectively. Figure 1a displays the directions of these force components, which can be identified through the sun-sail direction \hat{s} ; the unit vector normal to the sail having a positive component along \hat{s} (\hat{n}); the specular direction to \hat{s} with respect to \hat{n} ($\hat{\xi}$); and the tangent unit vector \hat{t} lying in the plane generated by \hat{s} and \hat{n} and defined as

$$\hat{t} := \frac{\hat{n} \times \hat{s}}{\|\hat{n} \times \hat{s}\|} \times \hat{n} = \frac{\hat{s} - \cos \beta \hat{n}}{\sin \beta}$$



a) Schematic representation

where β is the so-called solar-sail pitch angle defined as $\cos \beta = \hat{n} \cdot \hat{s}$. Note that based on the definition of \hat{n} , $\cos \beta$ is always nonnegative. As shown in the sketch of Fig. 1a, the force due to the incoming radiation f_a points along \hat{s} . The force provided by the specularly reflected radiation f_{rs} points along $\hat{\xi}$ and is caused by photons that are reflected symmetrically with respect to the normal of the sail, thus yielding an exchange of momentum. Diffuse reflection stems from the sail surface roughness, which causes photons to be uniformly reflected in all directions, yielding a component of the force toward the direction normal to the sail \hat{n} . Finally, as the absorbed photons are reradiated in all directions, the force f_e is generated, which is orthogonal to the sail surface and points again along \hat{n} .

Based on chapter 2 of Ref. [1], the unit vectors \hat{s} and $\hat{\xi}$ can be expressed in terms of \hat{n} and \hat{t} as

$$\begin{aligned} \hat{s} &= \cos \beta \hat{n} + \sin \beta \hat{t} \\ \hat{\xi} &= \cos \beta \hat{n} - \sin \beta \hat{t} \end{aligned}$$

so that the aforementioned forces can be expressed as [22]

$$\begin{aligned} f_a &= \varepsilon \cos \beta \hat{s} = \varepsilon \cos \beta (\cos \beta \hat{n} + \sin \beta \hat{t}) \\ f_{rs} &= \varepsilon \rho s \cos \beta \hat{\xi} = \varepsilon \rho s \cos \beta (\cos \beta \hat{n} - \sin \beta \hat{t}) \\ f_{ru} &= \varepsilon B_f \rho (1 - s) \cos \beta \hat{n} \\ f_e &= \varepsilon (1 - \rho) \frac{\varepsilon_f B_f - \varepsilon_b B_b}{\varepsilon_b + \varepsilon_f} \cos \beta \hat{n} \end{aligned} \quad (1)$$

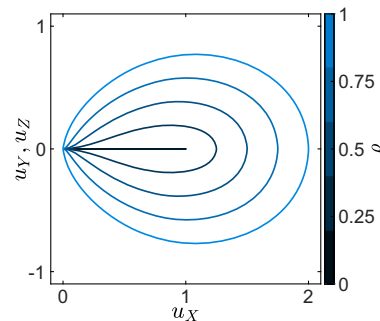
In Eq. (1), $\varepsilon = AP_{SR} \text{ m}^{-1}$, which combines optical and physical parameters of the sail and has small magnitude; $\rho \in [0, 1]$ is the fraction of reflected radiation to the total amount of radiation illuminating the sail; $s \in [0, 1]$ is the fraction of specularly reflected radiation to the total reflected radiation; ε_b and ε_f are the back and front surface emissivity coefficients, respectively; and B_b and B_f are back and front non-Lambertian coefficients, respectively. The SRP force is found as

$$f_{SRP} = f_a + f_{rs} + f_{ru} + f_e$$

B. Parametrization of the Control Set

Controlling the sail attitude (i.e., the normal vector \hat{n}) allows us to change the direction and magnitude of the resulting SRP. A reliable inference of optical coefficients is indeed mandatory to accurately estimate the mapping between \hat{n} and f_{SRP} .

To carry out controllability analysis, solar-sail dynamics is conveniently modeled as a nonlinear control-affine system (see



b) Control sets for different reflectivity coefficients and $s = 1$

Fig. 1 Components of the SRP force. In Fig. 1b, u_x is the projection of u towards \hat{s} , whereas u_y and u_z are orthogonal components.

Sec. II.C), where the control variable is homogeneous to the force vector, namely, $\mathbf{u} := (\mathbf{f}_{\text{SRP}}/\varepsilon)$. Control set $U \subset \mathbb{R}^3$ is then given by

$$U = \left\{ \mathbf{u} = \frac{\mathbf{f}_{\text{SRP}}(\hat{\mathbf{n}})}{\varepsilon}, \hat{\mathbf{n}} \in \mathbb{R}^3, \|\hat{\mathbf{n}}\| = 1 \right\}$$

Figure 1b shows the intersection of U on the plane generated by $\hat{\mathbf{n}}$ and $\hat{\mathbf{s}}$ for various optical properties. The set is a surface of revolution with axis $\hat{\mathbf{s}}$, and it is nonconvex unless $\rho = s = 1$. Note that the interior of the surface is not part of U . When reemitted radiation is neglected, which is most often a reasonable assumption for control purposes, U contains the origin but mapping between $\hat{\mathbf{n}}$ and \mathbf{u} is nonsmooth at this point. Two extreme cases can be identified: ideal sails are constituted by perfectly reflective surfaces ($\rho = s = 1$), whereas perfectly absorptive surfaces are the worst-case scenario ($\rho = 0$, with f_e neglected) because SRP is systematically parallel to $\hat{\mathbf{s}}$. Although sails are designed to be as close to ideal as possible, partial absorption of the energy is unavoidable in real-life applications; in addition, optical properties exhibit degradation with time. Hence, the fraction of reflected radiation decreases with the lifetime of the satellite, as was discussed in Refs. [20,23].

C. Equations of Motion

The controllability of a solar sail in orbit around a celestial body is considered in this study. The following assumptions are introduced:

1) The orbital period of the sail is much smaller than the one of the heliocentric orbit of the attractor so that variations of the sun direction $\hat{\mathbf{s}}$ over a single orbit of the sail are neglected.

2) Solar eclipses are neglected. Targeting a certification of non-controllability in Sec. III, this assumption is conservative because controllability can only deteriorate while including eclipses because no SRP can be generated in the shadow. Eclipses restrain the time period of control of the satellite. Moreover, as we highlighted before, our results are independent of the semimajor axis of the orbit, which has a major impact on the duration of eclipses during the orbital period. Therefore, in order to provide a conservative planet-independent and semimajor-axis-independent result, we suppose the sail is controlled over the whole orbital period.

3) Reemitted radiation is neglected. In fact, this component of SRP can be reasonably regarded as a disturbance for control purposes.

The equations of motion are written in a set of Keplerian-like orbital elements, which leverages the axial symmetry of the problem with respect to the sun's direction; namely, consider a reference frame \mathcal{S} with the origin at the center of the planet, the $\hat{\mathbf{X}}$ axis toward $\hat{\mathbf{s}}$, $\hat{\mathbf{Y}}$ lying in the plane of the planet's orbit around the sun and orthogonal to $\hat{\mathbf{X}}$, and $\hat{\mathbf{Z}}$ chosen to form a right-hand frame. Because this study focuses on short-time controllability (characteristic time is of the order of one orbital period), the motion of this frame is neglected by virtue of the first assumption given earlier in this paper. Figure 2 represents the vectors \mathbf{h} , \mathbf{e} , and $\hat{\mathbf{N}}$, which denote the angular momentum, the eccentricity, and the ascending node vectors, respectively. Let γ_1 , γ_2 , and γ_3 be Euler angles orienting the eccentricity vector according to an $\hat{\mathbf{X}}\text{-}\hat{\mathbf{Y}}\text{-}\hat{\mathbf{X}}$ rotation, as depicted in Fig. 2, so that γ_2 is the angle between the angular momentum of the orbit and the sun direction; and a , e , and f are the semimajor axes, eccentricity, and true anomaly, respectively. The motion of slow elements, $I = (\gamma_1, \gamma_2, \gamma_3, a, e)^T \in M$, where M is the configuration manifold, is governed by

$$\begin{aligned} \frac{dI}{dt} &= \varepsilon \sqrt{\frac{a(1-e^2)}{\mu}} G(I, f) R(I, f) \mathbf{u} \\ \frac{df}{dt} &= \omega(I, f) + \varepsilon F(I, f) R(I, f) \mathbf{u} \end{aligned} \quad (2)$$

where components of \mathbf{u} are in the reference frame \mathcal{S} ,

$$R(I, f) = R_X(\gamma_3 + f) R_Y(\gamma_2) R_X(\gamma_1)$$

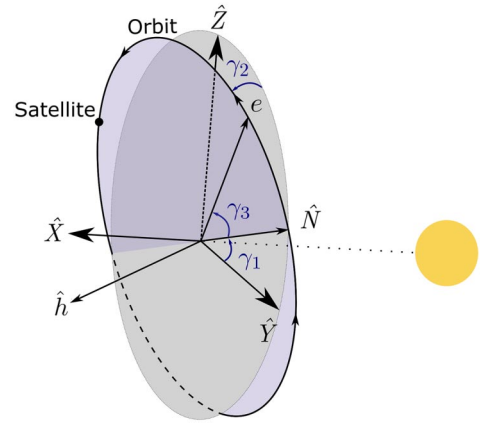


Fig. 2 Euler angles γ_i orienting the orbit according to a $\hat{\mathbf{X}}\text{-}\hat{\mathbf{Y}}\text{-}\hat{\mathbf{X}}$ rotation with respect to the reference frame \mathcal{S} . Here, \mathbf{h} and \mathbf{e} denote the angular momentum and eccentricity vectors.

is the rotation matrix from reference to the local-vertical/local-horizontal frames,[†]

$$\omega(I, f) = \sqrt{\frac{\mu}{a(1-e^2)^3}} (1 + e \cos f)^2$$

and both $F(I, f)$ and $G(I, f)$ can be deduced from the Gauss variational equations of the classical elements, where $G(I, f)$ is

$$G = \begin{pmatrix} 0 & 0 & \frac{\sin(\gamma_3 + f)}{\sin \gamma_2 (1 + e \cos f)} \\ 0 & 0 & \frac{\cos(\gamma_3 + f)}{1 + e \cos f} \\ -\frac{\cos f}{e} & \frac{2 + e \cos f \sin f}{1 + e \cos f} \frac{\sin f}{e} & \frac{\cos(\gamma_3 + f)}{1 + e \cos f} \\ \frac{2ae}{1-e^2} \sin f & \frac{2ae}{1-e^2} (1 + e \cos f) & 0 \\ \sin f & \frac{e \cos^2 f + 2 \cos f + e}{1 + e \cos f} & 0 \end{pmatrix}$$

The peculiar choice of Euler angles follows from the symmetry of system (2), namely, axial symmetry with respect to the axis $\hat{\mathbf{X}}$; and it has the main consequence that the controllability results in Sec. V are independent of γ_1 , which is a rotation about this axis. We also note that $(1 + e \cos f)G(I, f)R(I, f)$ is a trigonometric polynomial in f because eclipses were neglected. This has significant advantages for the numerical methodology detailed in Sec. IV.

Finally, orbital perturbations (other than SRP) are not included in Eq. (2) because we are interested in investigating geometric obstructions to the controllability of solar sails, regardless of their size.

III. Controllability of a Solar Sail

We are interested in studying obstructions to the controllability of solar sails in orbit about a celestial body. More precisely, we want to assess the existence of variations of the current orbital elements set that a sail cannot generate after a single orbital period.

The classical approach to inspect controllability of control-affine systems with periodic drift was detailed in Ref. [24] and chapter 4 of Ref. [25]. Specifically, global controllability (that is the existence of an admissible control steering the system from any initial point toward any target) is guaranteed, provided that the following sufficient conditions are met:

- 1) The drift of the system is periodic (or, more generally, recurrent).
- 2) The Lie algebra rank condition (LARC) holds; namely, the set of vector fields defining the control-affine system are bracket generating.
- 3) The convex hull of the control set U is a neighborhood of the origin in \mathbb{R}^5 .

[†]Here, $R_A(\phi)$ denotes the rotation matrix of angle ϕ about the axis $\hat{\mathbf{A}}$.

Keplerian motion satisfies the first condition. Two different cases are distinguished for the computation of the rank of the Lie algebra: First, *perfectly absorptive sails* (i.e., $\rho = 0$) are such that the control set degenerates to a segment aligned to \hat{s} , as shown in Fig. 1b. The Appendix offers a detailed evaluation of Lie brackets in this case, which shows that the algebra is rank deficient. This allows us to prove noncontrollability of the system and to deduce an integral of motion, namely, the projection of the angular momentum toward \hat{s} ([26] Chap. 12). Second, *real-life sails* are such that ρ is strictly positive and smaller than one. In this case, the control set is no longer degenerate and the system is bracket generating. Nevertheless, controllability of this system cannot be assessed because U does not contain the origin in its interior (the origin is on the boundary of the control set, as depicted in Fig. 1b) so that the third condition is not satisfied, and the classical approach cannot be used to investigate controllability of this system.

A novel sufficient condition relaxing the third requirement was proposed by the authors in Refs. [27,28]. According to that result, system (2) is controllable with respect to the slow variables, both globally (meaning that there exists an admissible control allowing to reach any final orbit from any initial one) and “locally in one period of the fast variable” (meaning that there is a neighborhood of the initial orbit that can be reached in no longer than one period of the initial orbit) if the control set U contains the origin (not necessarily in its topological interior), and if, for all I in M , the following condition holds:

$$\text{cone} \left\{ \frac{dI(f, I, \mathbf{u})}{dt}, \mathbf{u} \in U, f \in \mathbb{S}^1 \right\} = T_I M \quad (3)$$

where \mathbb{S}^1 denotes the unit circle so that $f \in [0, 2\pi]$, and $T_I M$ denotes the tangent space to the manifold M at point $I \in M$ (intuitively, $T_I M$ is the vector space made of the velocities of all curves passing through point I). Herebefore, the operator *cone* indicates the conical hull: for a subset A of a vector space, $\text{cone } A$ is the set of linear combinations with nonnegative coefficients of vectors of A ,

$$\text{cone } A = \left\{ \sum_{i=1}^k \lambda_i x_i, k \in \mathbb{N}, (\lambda_1, \dots, \lambda_k) \in [0, +\infty)^k, (x_1, \dots, x_k) \in A^k \right\}$$

It is always a convex pointed cone. If condition (3) only holds at one point, it remains true around it, and controllability in the corresponding neighborhood follows. Clearly, because of the periodicity of the free motion, the angular position determined by the true anomaly does not play any role; any initial/final longitude can be departed from/reached up to some additional time spent along the periodic initial/final orbit. This result does not have an exact converse, but we examine a condition that clearly contradicts condition (3). Clearly, condition (3) cannot hold if, for some orbit I_0 , there exists a nonzero covector $p_{I_0} \in T_{I_0}^* M$ ($T_{I_0}^* M$ is the dual of the vector space $T_{I_0} M$, i.e., the vector space of all linear maps $T_{I_0} M \rightarrow \mathbb{R}$) such that

$$\left\langle p_{I_0}, \frac{dI(f, I_0, \mathbf{u})}{dt} \right\rangle > 0, \quad f \in \mathbb{S}^1, \mathbf{u} \in \text{cone } U, \|\mathbf{u}\| = 1 \quad (4)$$

where $\langle \cdot, \cdot \rangle$ denotes duality between covectors and vectors (i.e., applying a linear form to a vector); note that $\mathbf{u} \in U$ [from condition (3)] has been replaced with $\mathbf{u} \in \text{cone } U$, $\|\mathbf{u}\| = 1$, which is a way to select a nonzero vector in each half-line from the origin containing an element of U ; the covector p_{I_0} represents a linear coordinate function that may only increase at first order. Because the strict inequality also holds, replacing I_0 by any I in a small enough neighborhood, condition (4) entails an obstruction to local controllability in the following sense: one can find a half-space of the neighborhood of I_0 where motion is forbidden (see Fig. 3) when starting from I_0 and staying in this neighborhood; in practice, this means that there is one function of the orbital elements (say, the semimajor axis) that the sail cannot decrease while remaining close to the original orbit (and if the thrust is small, one period is not long enough to go far). Orbits in the

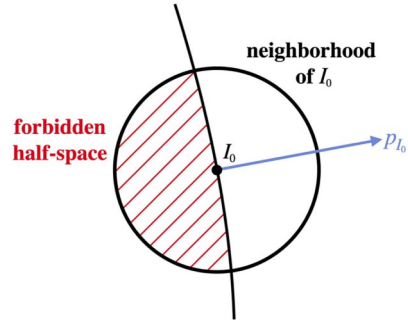


Fig. 3 Schematic representation of a half-space of the neighborhood of I_0 where motion is (locally) forbidden.

forbidden half-neighborhood might, however, be reached (i.e., global controllability could hold) but only by trajectories that must leave this neighborhood; in practice, this means that the sail we just mentioned could [even if condition (4) holds] be capable of decreasing its semimajor axis, but only at the price of first going “far” from the neighborhood of the initial orbit (by significantly increasing its inclination, for example).

For a detailed discussion on the gap between Eq. (4) and the negation of condition (3) for general control systems, we refer to the academic examples in section 2 of Ref. [28].

IV. Numerical Methodology to Inspect Local Controllability

Given some optical properties of the sail and orbital state I , we are interested in determining if Eq. (4) has any nontrivial solution $p_I \neq 0$. Two manipulations are introduced to facilitate this task.

First, let us denote

$$\tilde{G}(I, f) := (1 + e \cos f)G(I, f)R(I, f)$$

Therefore, the time derivative of I in Eq. (4) can be replaced as follows:

$$\frac{dI}{dt} = \frac{\varepsilon}{1 + e \cos f} \sqrt{\frac{a(1 - e^2)}{\mu}} \tilde{G}(I, f) \mathbf{u}$$

Because

$$\frac{\varepsilon}{1 + e \cos f} \sqrt{\frac{a(1 - e^2)}{\mu}}$$

is positive, $\tilde{G}(I, f) \mathbf{u}$ has the same sign as dI/dt ,

$$\frac{dI}{dt}$$

The fact that $\tilde{G}(I, f)$ is a quadratic trigonometric polynomial in f offers major benefits when positivity constraints are numerically enforced in Sec. IV.B. This operation has no impact on the sign of Eq. (4). We also note that system (2) is axially symmetric with respect to the sun–planet direction because it is independent of γ_1 and that the semimajor axis and planetary constant have no impact on the sign of Eq. (4). Hence, all outcomes of this controllability study are independent of both the semimajor axis and γ_1 (because of symmetry), and they are valid for any attractor (spherical symmetric central body) because the magnitude of SRP does not impact the noncontrollability condition (which is a geometric obstruction).

Second, the control set U is replaced by its conical hull $K_\alpha := \text{cone}(U)$, which is a cone of revolution of angle α , as illustrated in Fig. 4. This approximation makes the problem convex, which has a major advantage for numerical computation. Replacing U by K_α has no impact on the closure of the reachable set of the control system, as

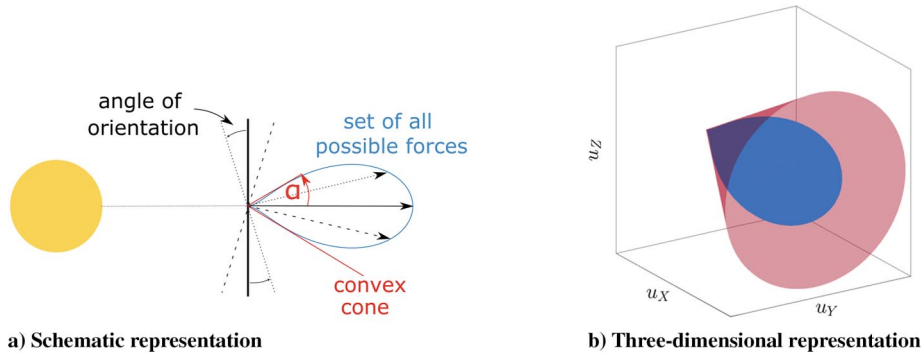


Fig. 4 Approximation of the control set (blue) by a convex cone (red).

discussed in Ref. [28]. Therefore, noncontrollability of the system with controls in K_α implies noncontrollability of the system with the original control set U . Neglecting thermal radiation (this simplification is not strictly necessary), cone angle α can be directly deduced from the optical properties of the sail introduced in Eq. (1). The relation is obtained by solving

$$\begin{aligned} \tan \alpha &= \max_{\beta \in [0, (\pi/2)]} \frac{\|(\mathbb{I} - \hat{s}\hat{s}^T)\mathbf{f}_{\text{SRP}}\|}{\mathbf{f}_{\text{SRP}} \cdot \hat{s}} \\ &= \max_{\beta \in [0, (\pi/2)]} \frac{\rho s \sin 2\beta + B_f \rho (1-s) \sin \beta}{1 + \rho s \cos 2\beta + B_f \rho (1-s) \cos \beta} \end{aligned} \quad (5)$$

This condition holds for

$$\beta^* = \cos^{-1} \left(\frac{-B_f \rho (1-s)(3\rho s + 1) + \sqrt{\kappa}}{8\rho s} \right)$$

with

$$\kappa = B_f^2 \rho^2 (1-s)^2 ((3\rho s - 1)^2 - 4\rho s) - 32\rho^2 s^2 (\rho s - 1)$$

where β^* denotes the solution of the maximization performed on the right-hand side of Eq. (5).

If $B_f = 0$, Eq. (5) simplifies to

$$\alpha(\rho, s) = \tan^{-1} \left(\frac{\rho s}{\sqrt{1 - \rho^2 s^2}} \right), \quad \rho s = \frac{\tan \alpha}{\sqrt{1 + \tan^2 \alpha}} \quad (6)$$

Hence, Eq. (4) is finally recast into

$$\begin{aligned} \exists p_I \in T_I^* M, p_I \neq 0 \text{ such that} \\ \langle p_I, \tilde{G}(I, f)\mathbf{u} \rangle > 0, \quad f \in \mathbb{S}^1, \mathbf{u} \in K_\alpha, \|\mathbf{u}\| = 1 \end{aligned} \quad (7)$$

A. Constructive Approach to Verify the Controllability Condition

A practical check of feasibility of problem (7) is carried out by solving the auxiliary optimization problem

$$\begin{aligned} \max_{J, \|p_I\| \leq 1} J \\ \text{subject to} \\ \langle p_I, \tilde{G}(I, f)\mathbf{u} \rangle \geq J, f \in \mathbb{S}^1, \mathbf{u} \in \partial K_\alpha, \|\mathbf{u}\| = 1 \end{aligned} \quad (8)$$

The constraint $\|p_I\| \leq 1$ is preferred to $\|p_I\| = 1$ to preserve convexity of problem (8). Problem (8) is convex and semi-infinite because inequality constraints need to be enforced on two infinite sets, namely, for all true anomalies between 0 and 2π and for all \mathbf{u} on the surface of the cone. Evaluating inequalities in the interior of the cone is not necessary because the dynamics are affine in \mathbf{u} . If J^* [which is the solution of problem (8)] is positive, problem (7) is verified: then, as discussed in the previous section, for the cone angle

α , there is an obstruction to local controllability around the orbit I . Conversely, when Eq. (3) holds at I , both J^* and the associated minimizer p_I must be zero.

A question of interest for mission design purposes is to identify minimal optical requirements that satisfy the necessary condition. This can be achieved by solving

$$\begin{aligned} \min_{\alpha} \alpha \\ \text{subject to} \\ J^*(\alpha) = 0 \end{aligned} \quad (9)$$

where $J^*(\alpha)$ denotes the solution of problem (8) for a given α . This angle can then be mapped into minimal requirements for the reflectivity of the sail via Eq. (6). Figure 5 provides an example of this process for a specific orbit (the detailed algorithm to achieve these solutions is provided in Sec. IV.B). The minimum cone angle solution of problem (9) (for the specific I used in this simulation) is emphasized with a diamond.

B. Optimization Problem

The numerical solution of problem (8) is achieved by using the formalism of positive trigonometric polynomials [18,19] to enforce positivity constraints for all values of f and \mathbf{u} without introducing any relaxation or discretization of the problem.

Let δ be an angle parametrizing control vectors on the surface of the cone, as shown in Fig. 6. Therefore, \mathbf{u} on the surface of the cone can be expressed as

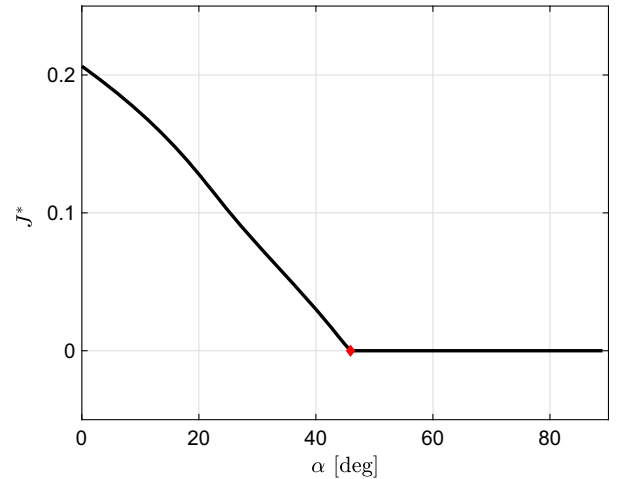


Fig. 5 Example of the solution of problems (8) (black curve) and (9) (red dot). Here, $\gamma_2 = 50$ deg, $\gamma_3 = 40$ deg, and $e = 0.7$.

**In practice, of course, the check can only be made at a single point, whereas the condition must hold for all I to ensure global controllability.

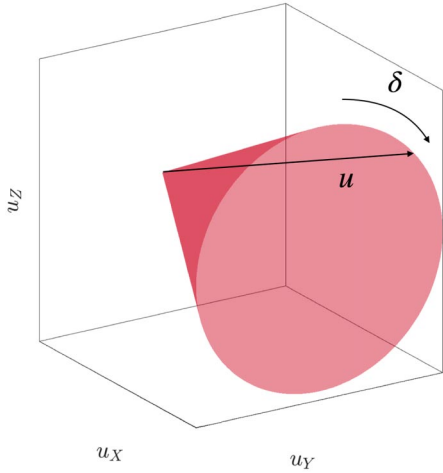


Fig. 6 Parametrization of the control vector.

$$\mathbf{u} = \begin{bmatrix} \cos \alpha \\ \cos \delta \sin \alpha \\ \sin \delta \sin \alpha \end{bmatrix}$$

According to Eq. (8), positivity of the following constraints must be verified:

$$p_l^T \tilde{G}(I, f) \mathbf{u} - J \geq 0 \quad f \in \mathbb{S}^1, \quad \mathbf{u} \in \partial K_\alpha \quad (10)$$

Inspection of $\tilde{G}(I, f) \mathbf{u}$ reveals that Eq. (10) is a bivariate trigonometric polynomial of degree two in f and the first degree in δ . Let $\langle \cdot, \cdot \rangle_H$ be the Hermitian product of two complex-valued vectors, i.e.,

$$\langle a, b \rangle_H = \langle \text{Re}(a), \text{Re}(b) \rangle + \langle \text{Im}(a), \text{Im}(b) \rangle$$

and denote

$$\begin{aligned} \Phi(f, \delta) &= \begin{bmatrix} 1, e^{i\delta} \end{bmatrix}^T \otimes \begin{bmatrix} 1, e^{if}, e^{2if} \end{bmatrix}^T \\ &= \begin{bmatrix} 1, e^{if}, e^{2if}, e^{i\delta}, e^{if} e^{i\delta}, e^{2if} e^{i\delta} \end{bmatrix}^T \end{aligned}$$

as the basis of the bivariate trigonometric polynomials of degree two in f and one in δ , respectively (here, \otimes denotes Kronecker's product). The left-hand term of Eq. (10) can be reformulated as

$$\begin{aligned} \langle p_l, \tilde{G}(I, f) \mathbf{u} \rangle - J &= p_l^T \left(\sum_{l=-1}^1 \sum_{k=-2}^2 \tilde{G}u^{(k,l)} e^{ikf} e^{il\delta} \right) - J \\ &= \langle \Phi(f, \delta), \tilde{G}u p_l - \mathbf{e}_1 J \rangle_H \end{aligned}$$

where $\tilde{G}u^{(k,l)}$ is the (k, l) -th coefficient of the Fourier transform^{††} of $\tilde{G}(I, f) \mathbf{u}$, and $\mathbf{e}_1 = [1, 0, 0, 0, 0, 0]^T$.

The formalism of the squared functional systems outlined in chapter 17 of Ref. [18] and chapter 3 of Ref. [19] allows us to recast the continuous positivity constraints into LMIs. The corresponding squared functional system of $\Phi(f, \delta)$ is $\mathcal{S}^2(f, \delta) = \Phi(f, \delta) \Phi^H(f, \delta)$, where $\Phi^H(f, \delta)$ denotes the conjugate transpose of $\Phi(f, \delta)$. Let N be the dimension of $\Phi(f, \delta)$ (six in our application); and $\Lambda_H: \mathbb{C}^N \rightarrow \mathbb{C}^{N \times N}$ is a linear operator mapping coefficients of polynomials in $\Phi(f, \delta)$ to the squared base so that application of Λ_H on $\Phi(f, \delta)$ yields

$$\Lambda_H(\Phi(f, \delta)) = \Phi(f, \delta) \Phi^H(f, \delta)$$

We define its adjoint operator $\Lambda_H^*: \mathbb{C}^{N \times N} \rightarrow \mathbb{C}^N$ as

$$\langle Y, \Lambda_H(\tilde{G}u) \rangle_H \equiv \langle \Lambda_H^*(Y), \tilde{G}u \rangle_H, \quad Y \in \mathbb{C}^{N \times N}, \quad \tilde{G}u \in \mathbb{C}^N$$

Theory of the squared functional systems postulated by Nesterov ([18] Chap. 17) proves that the trigonometric polynomial is non-negative if, and only if, a Hermitian positive semidefinite matrix Y exists such that $\tilde{G}u = \Lambda_H^*(Y)$. Dumitrescu extended this theory for multivariate trigonometric polynomials in chapter 3 of Ref. [19] and showed that all nonnegative bivariate trigonometric polynomials can be written as a sum of squares. This equivalence is false for three or more variables.

Thus, $\langle \Phi(f, \delta), \tilde{G}u \rangle_H$ is nonnegative for all $f \in \mathbb{S}^1$ and for all $\mathbf{u} \in K_\alpha$ if, and only if, a Hermitian positive semidefinite matrix Y exists such that $\tilde{G}u = \Lambda_H^*(Y)$, namely,

$$\langle \Phi(f, \delta), \tilde{G}u \rangle_H \geq 0, f \in \mathbb{S}^1, \mathbf{u} \in K_\alpha \Leftrightarrow \exists Y \geq 0: \tilde{G}u = \Lambda_H^*(Y)$$

In fact, it holds in this case that

$$\begin{aligned} \langle \Phi(f, \delta), \tilde{G}u \rangle_H &= \langle \Phi(f, \delta), \Lambda_H^*(Y) \rangle_H = \langle \Lambda_H(\Phi(f, \delta)), Y \rangle_H \\ &= \langle \Phi(f, \delta) \Phi^H(f, \delta), Y \rangle_H = \Phi^H(f, \delta) Y \Phi(f, \delta) \geq 0 \end{aligned}$$

For trigonometric polynomials, Λ^* is given by

$$\Lambda_H^*(Y) = \begin{bmatrix} \text{tr}(\langle Y, T_{00} \rangle) \\ \vdots \\ \text{tr}(\langle Y, T_{kl} \rangle) \\ \vdots \\ \text{tr}(\langle Y, T_{21} \rangle) \end{bmatrix} \quad k = 0, 1, 2, l = 0, 1$$

where $T_j, j = 0, 1, 2$ are the elementary Toeplitz matrices with ones on the j th diagonal and zeros elsewhere, and T_{kl} are obtained from a Kronecker product of such matrices, e.g.,

$$T_0 = \begin{pmatrix} 1 & 0 \\ 0 & 1 \end{pmatrix}, \quad T_1 = \begin{pmatrix} 0 & 1 & 0 \\ 0 & 0 & 1 \\ 0 & 0 & 0 \end{pmatrix},$$

$$T_{10} = T_0 \otimes T_1 = \begin{pmatrix} 0 & 1 & 0 & 0 & 0 & 0 \\ 0 & 0 & 1 & 0 & 0 & 0 \\ 0 & 0 & 0 & 0 & 0 & 0 \\ 0 & 0 & 0 & 0 & 1 & 0 \\ 0 & 0 & 0 & 0 & 0 & 1 \\ 0 & 0 & 0 & 0 & 0 & 0 \end{pmatrix}$$

Finally, the inequality in Eq. (10) is rewritten as an LMI:

$$\begin{aligned} \langle p_l, \tilde{G}(I, f) \mathbf{u} \rangle - J \geq 0, f \in \mathbb{S}^1, \mathbf{u} \in \partial K_\alpha &\Leftrightarrow \exists Y \geq 0 \\ \text{such that } \tilde{G}u p_l - \mathbf{e}_1 J &= \Lambda_H^*(Y) \end{aligned}$$

where $Y \in \mathbb{C}^{6 \times 6}$ is a Hermitian matrix to be determined. Hence, the finite-dimensional counterpart of problem (8) is

$$\begin{aligned} \min_{J, \|p_l\| \leq 1, Y \in \mathbb{C}^{6 \times 6}} J \\ \text{subject to} \\ Y \geq 0 \\ \Lambda_H^*(Y) = \tilde{G}u p_l - \mathbf{e}_1 J \end{aligned} \quad (11)$$

^{††}We note that $\tilde{G}^{kl} = \overline{\tilde{G}^{(-k,-l)}}$ because $\tilde{G}(I, f) \mathbf{u}$ is real valued.

Problem (11) consists of a convex programming with 27 design variables (scalar J , $p_I \in \mathbb{R}^5$, and $Y \in \mathbb{C}^{6 \times 6}$ symmetric), the ball constraint $|p_I| \leq 1$, and a single LMI of a 6×6 matrix. The computational time to solve this problem is extremely modest. Eventually, the solution of problem (9) is carried out by means of a simple bisection algorithm, which does not require the evaluation of derivatives of the nonsmooth function $J^*(\alpha)$ (we note that problem (8) has trivial solution $J = 0$ and $p_I = 0$ for $\alpha > \alpha_{\min}$). The CVX software [29,30] is used to solve convex problem (11). Fourier coefficients of $\tilde{G}(I, f)$, which is a second-degree trigonometric polynomial in f , are evaluated by means of the fast Fourier transform algorithm. We stress that there is no relaxation of problem (11) with respect to problem (8). Remarkably, enforcement of the constraint for all values of f and \mathbf{u} is exact and stems from the trigonometric nature of $\tilde{G}(I, f)\mathbf{u}$.

V. Application of the Methodology and Validation

A. Numerical Validation

A different algorithm for the evaluation of the necessary condition for local controllability of solar sails was proposed in Ref. [27]. In that case, controls necessary to move the sail toward the vertices of a simplex encompassing its current slow state were explicitly determined by solving a convex optimization problem. This was achieved by discretizing the control action with a finite number of generators of the convex cone and trigonometric polynomials in the mean anomaly. Figure 7 shows that the α_{\min} estimated with the algorithm in Ref. [27] for a specific orbit converges to the value obtained with the methodology presented in this paper as the degree of the trigonometric polynomials of the control action is increased. The estimation of Ref. [27] was conservative (namely, it overestimated α_{\min}) because an interior polyhedral approximation of the convex cone was used. We stress that the methodology outlined in Sec. IV outperforms the one in Ref. [27] because the exact solution of problem (8) is achieved by solving a low-dimensional convex program without any relaxation.

B. Minimal Optical Requirements

Figure 8 shows the minimum cone angle satisfying the condition as a function of γ_2 and γ_3 for various values of eccentricity (we recall that the semimajor axis and γ_1 have no influence on this angle). The minimal angle is symmetric with respect to $\gamma_2 = 90$ deg because

$$\langle p_I, \tilde{G}(e, \gamma_2, \gamma_3, f)\mathbf{u} \rangle = \langle -p_I, \tilde{G}(e, \pi - \gamma_2, \gamma_3, f)\mathbf{u} \rangle$$

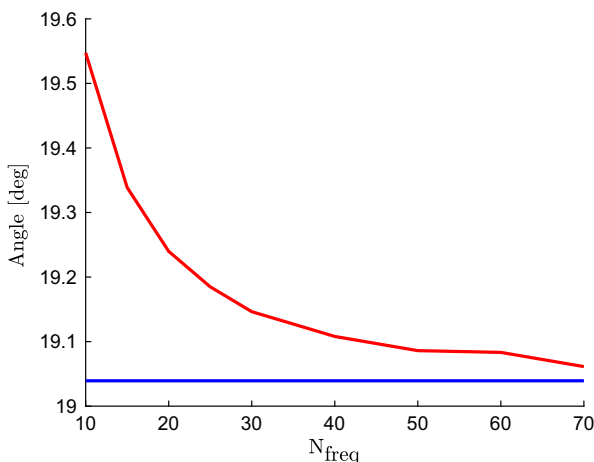


Fig. 7 Convergence of results obtained in Ref. [27] as a function of the number of harmonics used to estimate the control action (in red). Exact minimum angle obtained with methodology detailed in this paper (blue).

The solution is independent of γ_3 for circular orbits, as expected. Sensitivity with respect to γ_3 remains moderate, even for larger eccentricities. The minimal angle approaches zero as $\sin(\gamma_2) \rightarrow 0$. In this case, $\hat{\mathbf{s}}$ is aligned with the angular momentum of the orbit. On the other hand, for $\gamma_2 = 90$ deg, the sun is in the orbital plane.

Figures 9a and 9b represent α_{\min} as a function of γ_3 or γ_2 , respectively, for various values of eccentricity. The results confirm the strong dependency of α_{\min} on γ_2 and γ_3 for large eccentricity. Hence, the controllability of near-circular orbits requires more reflective sails with respect to high-eccentric orbits. Finally, we stress that the minimum angle α exists for all orbits, and it is systematically smaller than 90 deg, which means that the sail has not to be ideal (i.e. reflectivity coefficient ρ does not have to be equal to 1) to make system (2) controllable. To compare with a real solar sail, the optical properties of the NASA reference model [31] (designed to support the Near-Earth Asteroid Scout and Lunar Flashlight solar-sail missions) correspond to a cone angle of 58.6 deg. This value is sufficient to satisfy the proposed condition for most planet-centered orbits, except for highly inclined ones.

C. Stationkeeping Example

The determination of α_{\min} entails practical consequences in the design of solar-sail maneuvers by imposing minimal requirements on its reflectivity. For example, consider the scenario where a solar sail is used to carry out stationkeeping of a lunar orbiter. The objective is to maintain the sail in the proximity of the nominal orbit $I_{\text{ref}} = (150 \text{ deg}, 60 \text{ deg}, 0 \text{ deg}, 2R_{\text{Moon}}, 0.01)$, where R_{Moon} denotes the equatorial radius of the moon. Initial conditions are perturbed, and the motion of the sail is subject to nonspherical gravitational harmonics up to order and degree two. A simple local-optimal feedback controller that instantaneously minimizes the rate of change of the error function $e(t) = |I(t) - I_{\text{ref}}|$ is used to carry out the maneuver. The reference orbit has $\alpha_{\min} = 52$ deg, which corresponds to a minimum reflectivity coefficient of $\rho = 0.79$. Figures 10a and 10b depict the evolution of semimajor axis and error function for a poorly reflective sail and a highly reflective sail, namely, specular reflectivity equal to 0.5 and 0.9, respectively. At the beginning of the maneuver, both sails are able to decrease the error. This is because the direction of $I(t) - I_{\text{ref}}$ points inside the reachable half-space of the poorly reflective sail. Once $I(t) - I_{\text{ref}}$ is in the unreachable space, the poorly reflective sail starts drifting away from the reference, and its error function increases, whereas the highly reflective sail is able to keep its state in the proximity of I_{ref} . Because external perturbations are included, controllability of the highly reflective sail could be jeopardized if its surface-to-mass ratio is not large enough (20 m²/kg in this example), but the poorly reflective sail will not be able to stabilize the system, regardless of its size.

D. Comment on Heliocentric Orbits

Consider now a sail in a heliocentric orbit. This scenario can be a case for interplanetary transfers, for example. The same equations with two major corrections are used to model the problem. First, the rotation matrix R in Eq. (2) is removed because the local vertical/local horizontal frame is used, and $\hat{\mathbf{s}}$ is aligned with the radial direction. Moreover, the problem has central symmetry so that the results do not depend on any orbital element except for the eccentricity. For a perfectly absorptive solar sail, the dynamical system is not bracket generating because the control is radial, as proved in Ref. [32]. The integral of motion related to this rank deficiency is the magnitude of the angular momentum. For a nonideal sail, the system becomes bracket generating as soon as a tangential component appears: even for very weakly reflective sails.

Using the methodology of Sec. IV to solve the optimization problem indicates that even a very poorly reflective sail (i.e., $0 < \rho \ll 1$) is locally controllable over one orbital period. Specifically, the necessary condition is satisfied as soon as the sail is capable of producing even a weak force orthogonal to the radial vector. Therefore, the minimum cone angle α_{\min} approaches zero. However, interplanetary transfers are often envisaged on a fraction of a heliocentric orbit so that the proposed methodology is not very useful to

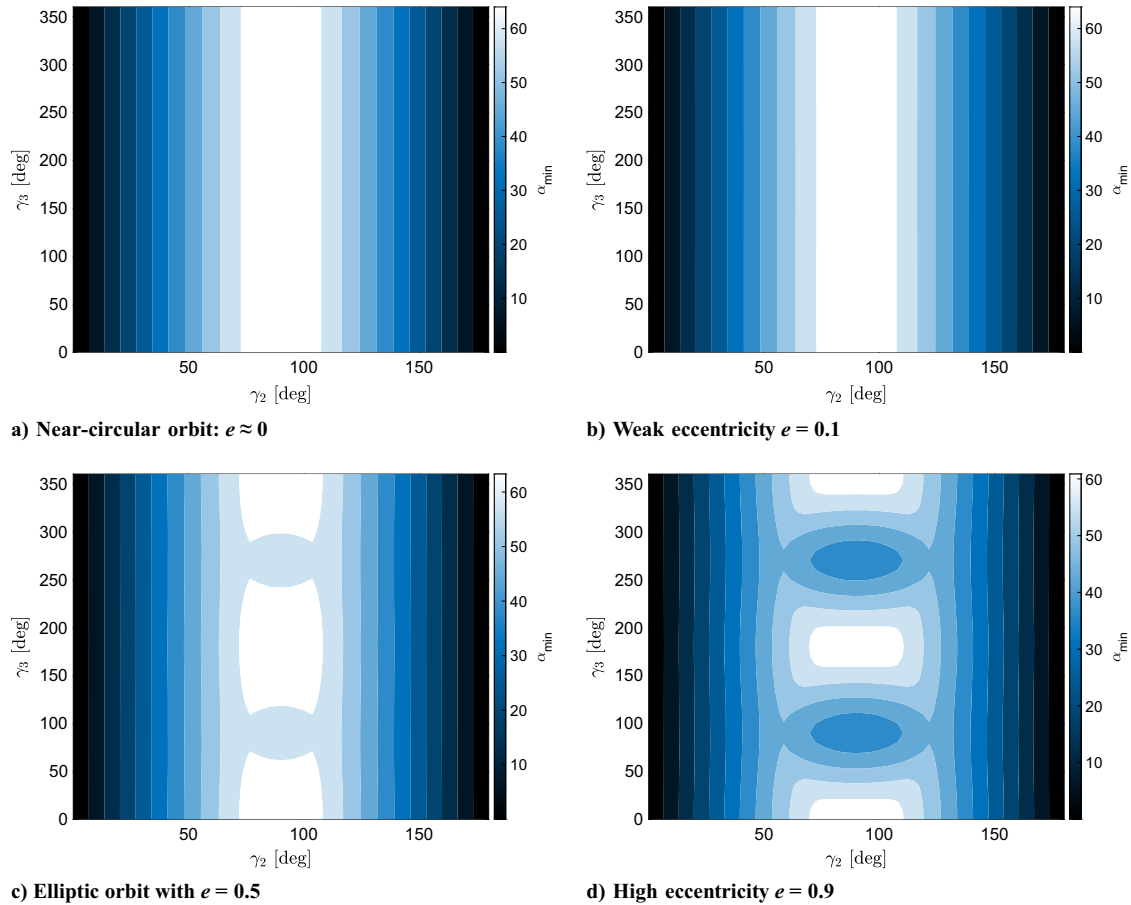


Fig. 8 Results for different planet-centered orbits.

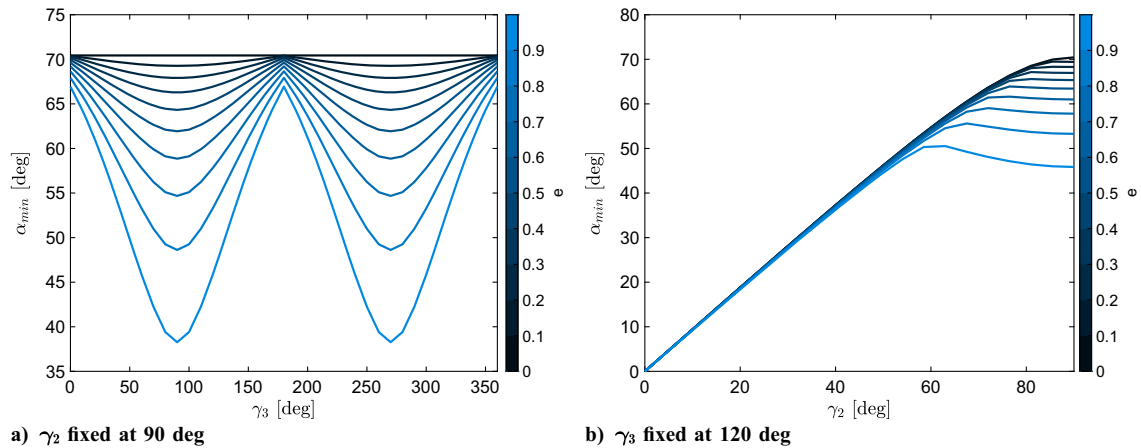


Fig. 9 Minimum cone angle as a function of Euler angles.

analyze mission scenarios of interplanetary transfers: any noncompletely absorptive sail yields a controllable system, but the time necessary to achieve maneuvers can be too long for this result to be of practical interest.

VI. Conclusions

This paper offers a novel methodology to assess the local controllability of nonideal solar sails in orbit around a celestial body. This is achieved by solving a semi-infinite convex optimization problem. Its solution is obtained by leveraging on both the formalism of bivariate polynomials and on the rational trigonometric

nature of Gauss variational equations, which limits the order of the polynomial for which the sign has to be evaluated. A failure of this requirement implies a certificate of noncontrollability; i.e., it indicates that a half-space of the neighborhood of the current state vector in the orbital element set is not locally accessible by maneuvering the sail. Extensive exploitation of this methodology reveals that a minimum reflectivity of the sail exists that satisfies the necessary condition for any orbit. A remarkable byproduct of this analysis is that local controllability properties hold universally (namely, regardless the planetary constant and the surface-to-mass ratio of the sail) for nonideal sails, provided that a sufficient amount of incoming radiation is reflected. This result has straightforward

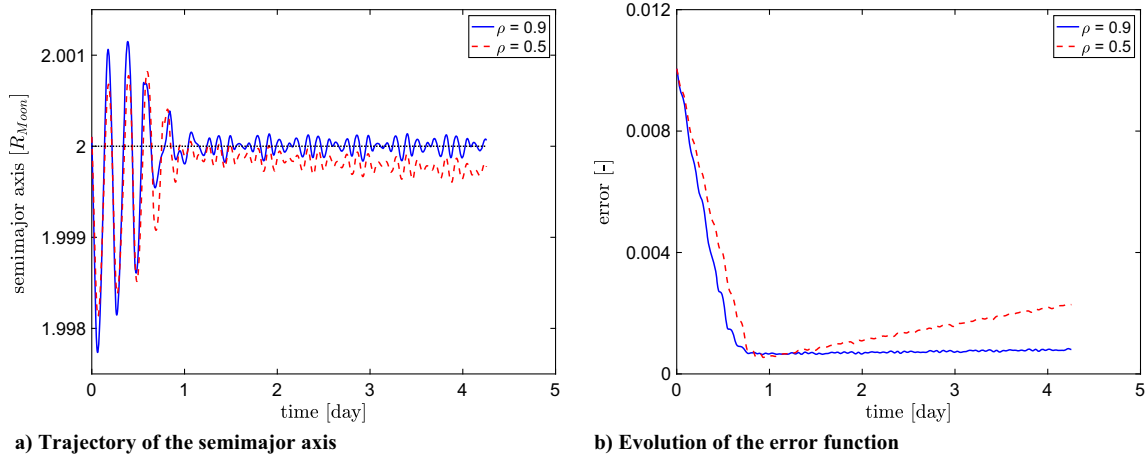


Fig. 10 Implementation of a stationkeeping algorithm using a locally optimal control law: reference value denoted by black dashed–dotted line.

implications in mission analysis of stationkeeping applications and transfer maneuvers with solar sails.

Appendix. Lie Brackets Computation for a Perfectly Absorptive Sail

Consider a control-affine dynamical system

$$\dot{x} = F^0(x) + \sum_{i=1}^m u_i F^i(x), \quad x \in \mathcal{M}, \quad \mathbf{u} = (u_1, \dots, u_m) \in U \subset \mathbb{R}^m \quad (\text{A1})$$

where \mathcal{M} is an n -dimensional manifold $F^i: \mathcal{M} \rightarrow T\mathcal{M}$ are smooth vector fields on \mathcal{M} . We note that Eq. (2) can be recast into the form of Eq. (A1) by choosing columns of $G(I, f)R(I, f)$ as vector fields F^i .

To compute Lie algebra, only the directions of the vector fields matter. To simplify, assume that the system to be controlled is given by a simple two-body equation with a term of perturbation aligned with an \hat{s} solar vector, which is considered fixed for a few orbits. For a perfectly absorptive solar sail, only the cross-sectional surface is controlled so that control is assumed to be $u \in [0, 1]$ with a certain coefficient ε defining SRP magnitude.

Using $x = (\mathbf{r}, \mathbf{v}) \in \mathbb{R}^6$ as the state vector, where \mathbf{r} and \mathbf{v} denote the Cartesian position and velocity vectors, respectively, a simple control-affine system can be rewritten as

$$\dot{x} = F^0(x) + \varepsilon u F^1(x)$$

with F^0 as the recurrent drift and F^1 as the SRP perturbation. Finally, the perturbed two-body problem is

$$\begin{cases} \frac{d\mathbf{r}}{dt} = \mathbf{v} \\ \frac{d\mathbf{v}}{dt} = -\frac{\mu}{r^3} \mathbf{r} + \varepsilon \hat{s} u \end{cases} \quad (\text{A2})$$

where $r = \|\mathbf{r}\|$. System (A2) provides two vector fields:

$$\begin{aligned} F^0 &= v_x \frac{\partial}{\partial r_x} + v_y \frac{\partial}{\partial r_y} + v_z \frac{\partial}{\partial r_z} - \frac{r_x}{r^3} \frac{\partial}{\partial v_x} - \frac{r_y}{r^3} \frac{\partial}{\partial v_y} - \frac{r_z}{r^3} \frac{\partial}{\partial v_z} \\ F^1 &= s_x \frac{\partial}{\partial v_x} + s_y \frac{\partial}{\partial v_y} + s_z \frac{\partial}{\partial v_z} \end{aligned}$$

To simplify, let us denote vector fields

$$\begin{aligned} v \frac{\partial}{\partial r} &= v_x \frac{\partial}{\partial r_x} + v_y \frac{\partial}{\partial r_y} + v_z \frac{\partial}{\partial r_z}, \\ \frac{r}{r^3} \frac{\partial}{\partial v} &= \frac{r_x}{r^3} \frac{\partial}{\partial v_x} + \frac{r_y}{r^3} \frac{\partial}{\partial v_y} + \frac{r_z}{r^3} \frac{\partial}{\partial v_z} \\ s \frac{\partial}{\partial v} &= s_x \frac{\partial}{\partial v_x} + s_y \frac{\partial}{\partial v_y} + s_z \frac{\partial}{\partial v_z} \end{aligned}$$

and

$$F^{sr} = s \frac{\partial}{\partial r}, \quad F^{rr} = r \frac{\partial}{\partial r}, \quad F^{vr} = v \frac{\partial}{\partial r}, \quad F^{sv} = s \frac{\partial}{\partial v}, \dots$$

Finally, by denoting $\hat{s} \cdot \mathbf{r}$ as a scalar product of two vectors, \hat{s} and \mathbf{r} , the computation of Lie brackets gives the following results:

$$\begin{aligned} F^0 &= v \frac{\partial}{\partial r} - \frac{r}{r^3} \frac{\partial}{\partial v} = F^{vr} - \frac{1}{r^3} F^{rv}, \quad F^1 = s \frac{\partial}{\partial v} = F^{sv}, \\ F^{01} &= [F^0, F^1] = -F^{sr} \\ F^{001} &= [F^0, [F^0, F^1]] = \frac{3(\hat{s} \cdot \mathbf{r})}{r^5} F^{rv} - \frac{F^{sv}}{r^3}, \quad F^{101} = [F^1, [F^0, F^1]] = 0 \\ F^{0001} &= [F^0, [F^0, [F^0, F^1]]] = \frac{1}{r^3} F^{sr} + \frac{3(\mathbf{v} \cdot \mathbf{r})}{r^5} F^{sv} \\ &\quad + \left(\frac{3(\hat{s} \cdot \mathbf{v})}{r^5} - \frac{15(\hat{s} \cdot \mathbf{r})(\mathbf{v} \cdot \mathbf{r})}{r^7} \right) F^{rv} + \frac{3(\hat{s} \cdot \mathbf{r})}{r^5} (F^{vv} - F^{rr}) \end{aligned}$$

All subsequent iterations are linear combinations of the previous vector fields. Thus, the Lie algebra of system (A2) has five independent vector fields if $\hat{s} \cdot \mathbf{r} \neq 0$:

$$F^{sr}, F^{sv}, F^{rv}, F^{vr}, F^{vv} - F^{rr}$$

$$\dim \text{Lie}(F^0, F^1, \dots) = 5 < \dim \mathbb{R}^6 = 6$$

Moreover, rank deficiency implies that an integral of motion exists, which happens to be the projection of the angular momentum \mathbf{h} toward \hat{s} , namely, $\hat{s} \cdot \mathbf{h} = \hat{s} \cdot (\mathbf{r} \times \mathbf{v}) = \det(\mathbf{r}, \mathbf{v}, \hat{s})$. In fact, the Lie derivative of $\hat{s} \cdot \mathbf{h}$ with respect to the controlled vector field

$$F^1 = s_x \frac{\partial}{\partial v_x} + s_y \frac{\partial}{\partial v_y} + s_z \frac{\partial}{\partial v_z}$$

is

$$\begin{aligned}
L_{F^1}(\det(\mathbf{r}, \mathbf{v}, \hat{\mathbf{s}})) &= s_X \frac{\partial}{\partial v_X} \det(\mathbf{r}, \mathbf{v}, \hat{\mathbf{s}}) + s_Y \frac{\partial}{\partial v_Y} \det(\mathbf{r}, \mathbf{v}, \hat{\mathbf{s}}) \\
&\quad + s_Z \frac{\partial}{\partial v_Z} \det(\mathbf{r}, \mathbf{v}, \hat{\mathbf{s}}) \\
&= s_X(-r_Y s_Z + r_Z s_Y) + s_Y(r_X s_Z - r_Z s_X) \\
&\quad + s_Z(-r_X s_Y + r_Y s_X) \\
&= 0
\end{aligned}$$

Acknowledgment

This work was partially supported by the ESA (contract no. 4000134950/21/NL/GLC/my).

References

- [1] McInnes, C. R., *Solar Sailing*, Springer, London, 1999, Chap. 2. <https://doi.org/10.1007/978-1-4471-3992-8>
- [2] Macdonald, M., McInnes, C., and Dachwald, B., “Heliocentric Solar Sail Orbit Transfers with Locally Optimal Control Laws,” *Journal of Spacecraft and Rockets*, Vol. 44, No. 1, 2007, pp. 273–276. <https://doi.org/10.2514/1.17297>
- [3] Carzana, L., Visser, P., and Heiligers, J., “Locally Optimal Control Laws for Earth-Bound Solar Sailing with Atmospheric Drag,” *Aerospace Science and Technology*, Vol. 127, Aug. 2022, Paper 107666. <https://doi.org/10.1016/j.ast.2022.107666>
- [4] Gong, S. P., Gao, Y.-F., and Li, J., “Solar Sail Time-Optimal Interplanetary Transfer Trajectory Design,” *Research in Astronomy and Astrophysics*, Vol. 11, No. 7, 2011, Paper 981. <https://doi.org/10.1088/1674-4527/11/8/010>
- [5] Dachwald, B., “Optimal Solar Sail Trajectories for Missions to the Outer Solar System,” *AIAA/AAS Astrodynamics Specialist Conference and Exhibit*, AIAA Paper 2004-5406, June 2004. <https://doi.org/10.2514/6.2004-5406>
- [6] Mengali, G., and Quarta, A., “Near-Optimal Solar-Sail Orbit-Raising from Low Earth Orbit,” *Journal of Spacecraft and Rockets*, Vol. 42, No. 9, 2005, pp. 954–958. <https://doi.org/10.2514/1.14184>
- [7] Colombo, C., Miguel Banos, N., and Gkolias, I., “Modulating Solar Sail Control for End-Of-life Disposal with Solar Sails,” *5th International Symposium on Solar Sailing*, Aachen, Germany, 2019, <https://re.public.polimi.it/handle/11311/1123523?mode=complete>.
- [8] Niccolai, L., Quarta, A., and Mengali, G., “Solar Sail Heliocentric Transfers with a Q-Law,” *Acta Astronautica*, Vol. 188, No. 11, 2021, pp. 352–361. <https://doi.org/10.1016/j.actaastro.2021.07.037>
- [9] Caruso, A., Bassetto, M., Mengali, G., and Quarta, A. A., “Optimal Solar Sail Trajectory Approximation with Finite Fourier Series,” *Advances in Space Research*, Vol. 67, No. 9, 2021, pp. 2834–2843. <https://doi.org/10.1016/j.asr.2019.11.019>
- [10] Peloni, A., Ceriotti, M., and Dachwald, B., “Solar-Sail Trajectory Design for a Multiple Near-Earth-Asteroid Rendezvous Mission,” *Journal of Guidance, Control, and Dynamics*, Vol. 39, No. 12, Dec. 2016, pp. 2712–2724. <https://doi.org/10.2514/1.g000470>
- [11] Peloni, A., Rao, A. V., and Ceriotti, M., “Automated Trajectory Optimizer for Solar Sailing (ATOSS),” *Aerospace Science and Technology*, Vol. 72, Jan. 2018, pp. 465–475. <https://doi.org/10.1016/j.ast.2017.11.025>
- [12] Kim, M., and Hall, C., “Symmetries in the Optimal Control of Solar Sail Spacecraft,” *Celestial Mechanics and Dynamical Astronomy*, Vol. 92, No. 8, 2005, pp. 273–293. <https://doi.org/10.1007/s10569-004-2530-x>
- [13] Sullo, N., Peloni, A., and Ceriotti, M., “Low-Thrust to Solar-Sail Trajectories: A Homotopic Approach,” *Journal of Guidance, Control, and Dynamics*, Vol. 40, No. 11, Nov. 2017, pp. 2796–2806. <https://doi.org/10.2514/1.g002552>
- [14] Niccolai, L., Quarta, A. A., and Mengali, G., “Analytical Solution of the Optimal Steering Law for Non-Ideal Solar Sail,” *Aerospace Science and Technology*, Vol. 62, March 2017, pp. 11–18. <https://doi.org/10.1016/j.ast.2016.11.031>
- [15] Song, Y., and Gong, S., “Solar Sail Trajectory Optimization of Multi-Asteroid Rendezvous Mission,” *Acta Astronautica*, Vol. 157, April 2019, pp. 111–122. <https://doi.org/10.1016/j.actaastro.2018.12.016>
- [16] Caruso, A., Mengali, G., Quarta, A. A., and Niccolai, L., “Solar Sail Optimal Control with Solar Irradiance Fluctuations,” *Advances in Space Research*, Vol. 67, No. 9, May 2021, pp. 2776–2783. <https://doi.org/10.1016/j.asr.2020.05.037>
- [17] Pellegrino, M., and Scheeres, D. J., “Reachability of a Passive Solar Sail in Earth Orbit,” *Journal of Guidance, Control, and Dynamics*, Vol. 44, No. 2, Feb. 2021, pp. 360–369. <https://doi.org/10.2514/1.g005264>
- [18] Nesterov, Y., “Squared Functional Systems and Optimization Problems,” *High Performance Optimization*, edited by P. M. Pardalos, D. Hearn, H. Frenk, K. Roos, T. Terlaky, and S. Zhang, Vol. 33, Applied Optimization, Springer, Boston, MA, 2000, pp. 405–440, Chap. 17. https://doi.org/10.1007/978-1-4757-3216-0_17
- [19] Dumitrescu, B., *Positive Trigonometric Polynomials and Signal Processing Applications*, Springer, Berlin, 2007, Chap. 3. <https://doi.org/10.1007/978-1-4020-5125-8>
- [20] Dachwald, B., Macdonald, M., McInnes, C. R., Mengali, G., and Quarta, A. A., “Impact of Optical Degradation on Solar Sail Mission Performance,” *Journal of Spacecraft and Rockets*, Vol. 44, No. 4, July 2007, pp. 740–749. <https://doi.org/10.2514/1.21432>
- [21] Montenbruck, O., and Gill, E., *Satellite Orbits*, Springer Science + Business Media, Berlin, 2000, Chap. 3. <https://doi.org/10.1007/978-3-642-58351-3>
- [22] Rios-Reyes, L., and Scheeres, D. J., “Generalized Model for Solar Sails,” *Journal of Spacecraft and Rockets*, Vol. 42, No. 1, Jan. 2005, pp. 182–185. <https://doi.org/10.2514/1.9054>
- [23] Niccolai, L., Quarta, A. A., and Mengali, G., “Trajectory Approximation of a Solar Sail with Constant Pitch Angle and Optical Degradation,” *IEEE Transactions on Aerospace and Electronic Systems*, Vol. 58, No. 4, Aug. 2022, pp. 3643–3649. <https://doi.org/10.1109/taes.2021.3124867>
- [24] Bonnard, B., “Contrôlabilité des Systèmes non Linéaires,” *Comptes Rendus de l’Académie des Sciences—Series I—Mathematics*, Vol. 292, No. 10, 1981, pp. 535–537.
- [25] Jurdjevic, V., *Geometric Control Theory*, 1st ed., Cambridge Univ. Press, Cambridge, England, U.K., 1996, Chap. 4. <https://doi.org/10.1017/CBO9780511530036>
- [26] Scheeres, D. J., *Orbital Motion in Strongly Perturbed Environments*, Springer, Berlin, 2012, Chap. 12. <https://doi.org/10.1007/978-3-642-03256-1>
- [27] Herasimenka, A., Caillau, J., Dell’Elce, L., and Pomet, J., “Controllability Test for Fast-Oscillating Systems with Constrained Control. Application to Solar Sailing,” *2022 European Control Conference (ECC)*, Inst. of Electrical and Electronics Engineers, New York, 2022, pp. 2143–2148. <https://doi.org/10.23919/ECC5457.2022.9838146>
- [28] Caillau, J.-B., Dell’Elce, L., Herasimenka, A., and Pomet, J.-B., “On the Controllability of Nonlinear Systems with a Periodic Drift,” Preprint, submitted 15 Dec. 2022, <https://hal.inria.fr/hal-03779482>.
- [29] Grant, M., and Boyd, S., CVX: Matlab Software for Disciplined Convex Programming, Software Package, Ver. 2.1,” CVX Research, March 2014, <http://cvxr.com/cvx> [retrieved 6 Jan. 2020].
- [30] Grant, M., and Boyd, S., “Graph Implementations for Nonsmooth Convex Programs,” *Recent Advances in Learning and Control*, Lecture Notes in Control and Information Sciences, edited by V. Blondel, S. Boyd, and H. Kimura, Springer, Berlin, 2008, pp. 95–110, https://web.stanford.edu/~boyd/papers/pdf/graph_dcp.pdf [retrieved 6 Jan. 2020].
- [31] Heaton, A. F., and Artusio-Glimpse, A., “An Update to the NASA Reference Solar Sail Thrust Model,” *AIAA SPACE 2015 Conference and Exposition*, AIAA Paper 2015-4506, Aug. 2015. <https://doi.org/10.2514/6.2015-4506>
- [32] Bonnard, B., Caillau, J.-B., and Trélat, E., “Geometric Optimal Control of Elliptic Keplerian Orbits,” *Discrete and Continuous Dynamical Systems—B*, Vol. 5, No. 4, 2005, pp. 929–956. <https://doi.org/10.3934/dcdsb.2005.5.929>